Available online at www.sciencedirect.com
ScienceDirect
International Journal of Heat and Mass Transfer 50 (2007) 1388–1396
International Journal of HEAT and MASS TRANSFER
www.elsevier.com/locate/ijhmt

Three-dimensional linear stability of natural convection in horizontal concentric annuli

Takahiro Adachi *, Satoru Imai

Department of Mechanical Engineering, Akita University, 1-1 Tegata-Gakuen, Akita 010-8502, Japan

Received 12 April 2006; received in revised form 9 August 2006
Available online 8 December 2006

Abstract

We have performed three-dimensional linear stability analyses of natural convection of air ($Pr = 0.71$) in horizontal annuli between concentric cylinders by using a spectral element method. A linear stability theory is applied to a basic two-dimensional steady solution which is called a crescent-shaped convection, and an eigenvalue problem of matrix form is constituted. We evaluate a critical Rayleigh number where the basic flow loses its stability with respect to three-dimensional disturbances over a wide range of aspect ratio ($1 \leqslant A \leqslant 20$). It is found that the instability mode which destabilizes the basic convection exchanges among three different modes, and the new transition lines are proposed.

Keywords: Linear stability; Natural convection; Spectral element method; Critical Rayleigh number; Concentric annuli; Eigenvalue problem

1. Introduction

Natural convection in an annulus between two horizontal concentric cylinders has been extensively investigated because of its wide variety of practical and technical applications such as heat exchangers, thermal storage systems and electric transmission cables. The convective flow patterns in the annulus, where the temperature of the inner cylinder is kept higher than that of the outer cylinder, greatly depend on a aspect ratio A, which is defined as the ratio of the diameter of the inner cylinder to the gap width, and show rich transient phenomenon. Therefore, the natural convection in the annulus has also attracted theoretical attention to stabilities in order to clarify the mechanism of the transitions of the flow patterns.

Many experimental and numerical investigations have been conducted to study the natural convection in horizontal annuli [1–4]. Powe et al. [2] have performed flow visualizations of the natural convection of air ($Pr = 0.71$) and presented a following comprehensive description of different flow regimes depending on a parameter space of (Ra, A), where Ra is the Rayleigh number. Steady two-dimensional convections with two global circulations opposed symmetrically with the vertical center-plane were observed at relatively small values of the Rayleigh number, which is often called a crescent-shaped convection. As the Rayleigh number increased above a critical value, different flow patterns were found to occur depending on the aspect ratio. In the range of the aspect ratio $A < 2.8$, the steady crescent-shaped convection underwent a transition to an unsteady two-dimensional convection due to instability, which was characterized by periodic oscillations passing through the vertical center-plane at the top region of the annulus. For $2.8 < A < 8.5$, an oscillatory convection occurred above a critical Rayleigh number, which was characterized by a three-dimensional spiral motion in the upper portion of the annulus. For $A > 8.5$, a two-dimensional multicellular convection appeared.

However, another two-dimensional solution different from the crescent-shaped one has been found by Yoo [5] numerically, which had a flow pattern with two additional smaller vortices in the top region of the annulus as well as two large circulations similar to the crescent-shaped

* Corresponding author. Tel.: +81 18 889 2306; fax: +81 18 837 0405.
E-mail address: adachi@ipc.akita-u.ac.jp (T. Adachi).

0017-9310/$ - see front matter © 2006 Elsevier Ltd. All rights reserved.
doi:10.1016/j.ijheatmasstransfer.2006.09.029

Nomenclature

A	aspect ratio of the inner cylinder diameter to gap width, $A = 2r_i^*/L^*$
g^*	gravitational acceleration
h_m	Lagrange interpolants through Gauss–Legendre–Lobatto points
L^*	gap width of the annulus, representative length, $L^* = r_o^* - r_i^*$
l	wave length in the z-direction, $l = 2\pi/\alpha$
N	truncation parameter of expansions
p	pressure
Pr	Prandtl number, $Pr = \nu^*/\kappa^*$
r_i^*	radius of the inner cylinder
r_o^*	radius of the outer cylinder
(r, θ, z)	components of the location in the cylindrical co-ordinates
t	time
T	temperature
T_i^*	temperature of the inner cylinder
T_o^*	temperature of the outer cylinder
Ra	Rayleigh number, $Ra = \beta^* g^* (T_i^* - T_o^*) L^{*3}/(\nu^* \kappa^*)$
(u_r, u_θ, u_z)	components of the velocity of the cylindrical co-ordinates

Greek symbols

α	wave number in the z-direction
β^*	thermal expansion coefficient
ϵ	penalty number
κ^*	thermal diffusivity
λ^*	thermal conductivity
ν^*	kinematic viscosity
ρ^*	density
ω	eigenvalue, $\omega = \omega_r + i\omega_i$

Subscripts

$*$	dimensional value
c	critical

convection. Mizushima et al. [6] have calculated the bifurcation diagram of the two different solutions under the assumption of the two-dimensionality and clarified the origins of the change of the flow patterns due to the saddle-node bifurcation for small aspect ratios. Namely, they found the convection which had a saddle-node point in addition to the crescent-shaped convection. It should be noted that, in general, the crescent-shaped convection can be attained from natural initial conditions, while the convection with the saddle-node point can only be realized under the particular conditions and has less physical reality than the crescent-shaped convection.

Choi and Kim [7] have studied the linear stability of the crescent-shaped convection, which is physically more realizable, by solving the linear equations for three-dimensional disturbances with time marching method. It was shown that the principle of exchange of stabilities was valid for $A > 2.1$. This implied that the resultant three-dimensional spiral convection was a steady-state flow, which was in contrast to the previous findings of Powe et al. [2]. On the other hand, for $A < 2.1$, they could not find any critical Rayleigh number. Moreover, the three-dimensional linear stability theory for classical parallel flows has been applied by Dyko et al. [8]. They studied an end-wall effect on the instability and evaluated the critical Rayleigh numbers even for $A < 2.1$. They, however, always assumed the symmetry conditions at the vertical center-plane, which might not lead to realistic solutions especially for the small aspect ratio. In fact, Labonia and Guj [9] as well as Powe et al. [2] have recently performed an experimental study of the transition from steady to chaotic flow in a horizontal annulus for a small aspect ratio and showed an oscillating flow pattern passing through the vertical center-plane above a critical value.

In this way, the critical condition is not clear in the range of small aspect ratios. Therefore, we investigate the linear stability of the natural convection in an annulus focusing on the crescent-shaped convection and taking account of asymmetry conditions as well as symmetry ones at the vertical center-plane, and clarify the critical conditions. The three-dimensional linear stability theory is applied to the two-dimensional crescent-shaped convection by using a spectral element method. The eigenvalue problem of matrix form is constituted based on the linear stability theory. We evaluate the critical Rayleigh number where the two-dimensional convection loses the stability to the three-dimensional disturbances.

2. Mathematical formulation

2.1. Basic equations

Consider a fluid contained in a horizontal annulus between two infinitely long concentric cylinders with inner and outer radii r_i^* and r_o^* which are maintained at temperatures T_i^* and $T_o^* (< T_i^*)$, respectively. Fig. 1 shows the geometry of the annulus and co-ordinates system, where r^* is taken along the radial direction, θ is measured clockwise from the top of the vertical center-plane and z^*-axis is taken along the axis of the annulus with origin O.

We define non-dimensional quantities as follows:

$$r = \frac{r^*}{L^*}, \quad z = \frac{z^*}{L^*}, \quad u_r = \frac{u_r^*}{(\kappa^*/L^*)}, \quad u_\theta = \frac{u_\theta^*}{(\kappa^*/L^*)},$$
$$u_z = \frac{u_z^*}{(\kappa^*/L^*)}, \quad t = \frac{t^*}{(L^{*2}/\kappa^*)}, \quad p = \frac{p^*}{(\rho^* \kappa^*/L^{*2})}, \tag{1}$$
$$T = \frac{T^* - T_o^*}{T_i^* - T_o^*},$$

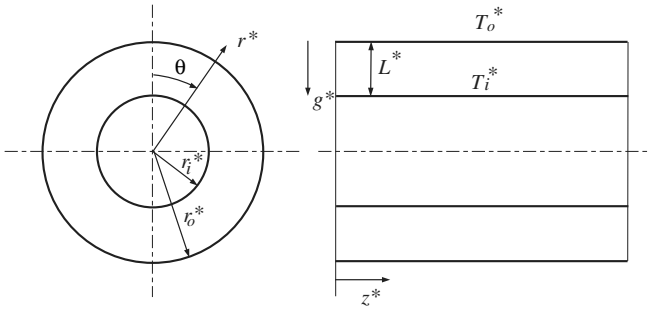

Fig. 1. Geometry and co-ordinate of the problem.

where L^*, κ^* and ρ^* are the gap width of the annulus, the coefficient of thermal diffusivity and the density of the fluid, respectively. We represent physical quantities with their dimensions by attaching a superscript * to them.

We assume that the flow is incompressible and the Boussinesq approximation is valid, where the approximation is applicable for sufficiently small temperature difference between the inner and outer cylinders. The velocity (u_r, u_θ, u_z), pressure p and temperature T are governed by the continuity, Navier–Stokes and energy equations as

$$\frac{\partial}{\partial r}(ru_r) + \frac{\partial u_\theta}{\partial \theta} + r\frac{\partial u_z}{\partial z} = 0, \tag{2}$$

$$\frac{\partial u_r}{\partial t} + u_r\frac{\partial u_r}{\partial r} + \frac{u_\theta}{r}\frac{\partial u_r}{\partial \theta} + u_z\frac{\partial u_r}{\partial z} - \frac{u_\theta^2}{r} = -\frac{\partial p}{\partial r} + PrRaT\cos\theta + Pr\left(\frac{\partial^2 u_r}{\partial r^2} + \frac{1}{r}\frac{\partial u_r}{\partial r} + \frac{1}{r^2}\frac{\partial^2 u_r}{\partial \theta^2} + \frac{\partial^2 u_r}{\partial z^2} - \frac{2}{r^2}\frac{\partial u_\theta}{\partial \theta} - \frac{u_r}{r^2}\right), \tag{3}$$

$$\frac{\partial u_\theta}{\partial t} + u_r\frac{\partial u_\theta}{\partial r} + \frac{u_\theta}{r}\frac{\partial u_\theta}{\partial \theta} + u_z\frac{\partial u_\theta}{\partial z} + \frac{u_r u_\theta}{r} = -\frac{1}{r}\frac{\partial p}{\partial \theta} - PrRaT\sin\theta + Pr\left(\frac{\partial^2 u_\theta}{\partial r^2} + \frac{1}{r}\frac{\partial u_\theta}{\partial r} + \frac{1}{r^2}\frac{\partial^2 u_\theta}{\partial \theta^2} + \frac{\partial^2 u_\theta}{\partial z^2} + \frac{2}{r^2}\frac{\partial u_r}{\partial \theta} - \frac{u_\theta}{r^2}\right), \tag{4}$$

$$\frac{\partial u_z}{\partial t} + u_r\frac{\partial u_z}{\partial r} + \frac{u_\theta}{r}\frac{\partial u_z}{\partial \theta} + u_z\frac{\partial u_z}{\partial z} = -\frac{\partial p}{\partial z} + Pr\left(\frac{\partial^2 u_z}{\partial r^2} + \frac{1}{r}\frac{\partial u_z}{\partial r} + \frac{1}{r^2}\frac{\partial^2 u_z}{\partial \theta^2} + \frac{\partial^2 u_z}{\partial z^2}\right), \tag{5}$$

$$\frac{\partial T}{\partial t} + u_r\frac{\partial T}{\partial r} + \frac{u_\theta}{r}\frac{\partial T}{\partial \theta} + u_z\frac{\partial T}{\partial z} = \frac{\partial^2 T}{\partial r^2} + \frac{1}{r}\frac{\partial T}{\partial r} + \frac{1}{r^2}\frac{\partial^2 T}{\partial \theta^2} + \frac{\partial^2 T}{\partial z^2}. \tag{6}$$

The flow field is characterized by three non-dimensional parameters, i.e., the Rayleigh number, Prandtl number and aspect ratio of the annulus, which are defined as

$$Ra = \frac{\beta^* g^* L^{*3}(T_i^* - T_o^*)}{\kappa^* \nu^*}, \quad Pr = \frac{\nu^*}{\kappa^*}, \quad A = \frac{2r_i^*}{L^*}, \tag{7}$$

where β^*, ν^* are the coefficients of thermal expansion and kinematic viscosity of the fluid, and g^* gravitational acceleration, respectively. It should be noted that the value of the Prandtl number is fixed as $Pr = 0.71$ (air) throughout this paper.

We assume that the surfaces of inner and outer cylinders are rigid and maintained at different uniform temperatures. Then the boundary conditions are written as

$$u_r = u_\theta = u_z = 0, \quad T = 1 \quad \text{at } r = \frac{A}{2}, \tag{8}$$

$$u_r = u_\theta = u_z = 0, \quad T = 0 \quad \text{at } r = \frac{A}{2} + 1. \tag{9}$$

2.2. Non-linear steady-state and linear disturbance equations

We calculate a non-linear steady-state solution to study its linear stability. In order to simplify the mathematical formulation, we introduce a penalty-function method, where the divergence-free condition of Eq. (2) is reduced to express a limiting state in which the divergence of the velocity is not zero but extremely small [10,11]. Then, the pressure p is replaced as

$$p = -\frac{1}{\epsilon}\left\{\frac{\partial}{\partial r}(ru_r) + \frac{\partial u_\theta}{\partial \theta} + r\frac{\partial u_z}{\partial z}\right\}, \tag{10}$$

where ϵ is a penalty number of order $O(10^{-8})$.

Now we focus on the two-dimensional crescent-shaped convection persistent in the axial z-direction of the annulus. Therefore, the non-linear steady-state solution is expressed as $(U_r(r,\theta), U_\theta(r,\theta), T(r,\theta))$. Substituting the expressions into Eqs. (2)–(6) and dropping the terms including the operator $\partial/\partial t$, we obtain the following two-dimensional steady-state equations as

$$U_r\frac{\partial U_r}{\partial r} + \frac{U_\theta}{r}\frac{\partial U_r}{\partial \theta} - \frac{U_\theta^2}{r} = \frac{1}{\epsilon}\frac{\partial}{\partial r}\left\{\frac{\partial}{\partial r}(rU_r) + \frac{\partial U_\theta}{\partial \theta}\right\} + PrRaT\cos\theta + Pr\left(\frac{\partial^2 U_r}{\partial r^2} + \frac{1}{r}\frac{\partial U_r}{\partial r} + \frac{1}{r^2}\frac{\partial^2 U_r}{\partial \theta^2} - \frac{2}{r^2}\frac{\partial U_\theta}{\partial \theta} - \frac{U_r}{r^2}\right), \tag{11}$$

$$U_r\frac{\partial U_\theta}{\partial r} + \frac{U_\theta}{r}\frac{\partial U_\theta}{\partial \theta} + \frac{U_r U_\theta}{r} = \frac{1}{\epsilon r}\frac{\partial}{\partial \theta}\left\{\frac{\partial}{\partial r}(rU_r) + \frac{\partial U_\theta}{\partial \theta}\right\} - PrRaT\sin\theta + Pr\left(\frac{\partial^2 U_\theta}{\partial r^2} + \frac{1}{r}\frac{\partial U_\theta}{\partial r} + \frac{1}{r^2}\frac{\partial^2 U_\theta}{\partial \theta^2} + \frac{2}{r^2}\frac{\partial U_r}{\partial \theta} - \frac{U_\theta}{r^2}\right), \tag{12}$$

$$U_r\frac{\partial T}{\partial r} + \frac{U_\theta}{r}\frac{\partial T}{\partial \theta} = \frac{\partial^2 T}{\partial r^2} + \frac{1}{r}\frac{\partial T}{\partial r} + \frac{1}{r^2}\frac{\partial^2 T}{\partial \theta^2}. \tag{13}$$

The boundary conditions for (U_r, U_θ, T) are the same as Eqs. (8) and (9). In addition, we assume that the steady-state flow does not pass through the vertical center-plane and is symmetric with it. Then, the symmetry condition is written as

$$\frac{\partial U_r}{\partial \theta} = U_\theta = \frac{\partial T}{\partial \theta} = 0 \quad \text{at } \theta = 0, \pi. \tag{14}$$

All the steady-state crescent-shaped solutions obtained from Eqs. (11)–(13) are not stable but become unstable due to instability, and undergo transitions to other flow patterns. We investigate the linear stability of the steady-state solutions by adding small disturbances to them and by observing the time dependence of the disturbances. Then, the velocity and temperature are expressed as the sum of the steady solution (U_r, U_θ, T) and the disturbances ($\hat{u}_r, \hat{u}_\theta, \hat{u}_z, \hat{T}$) as

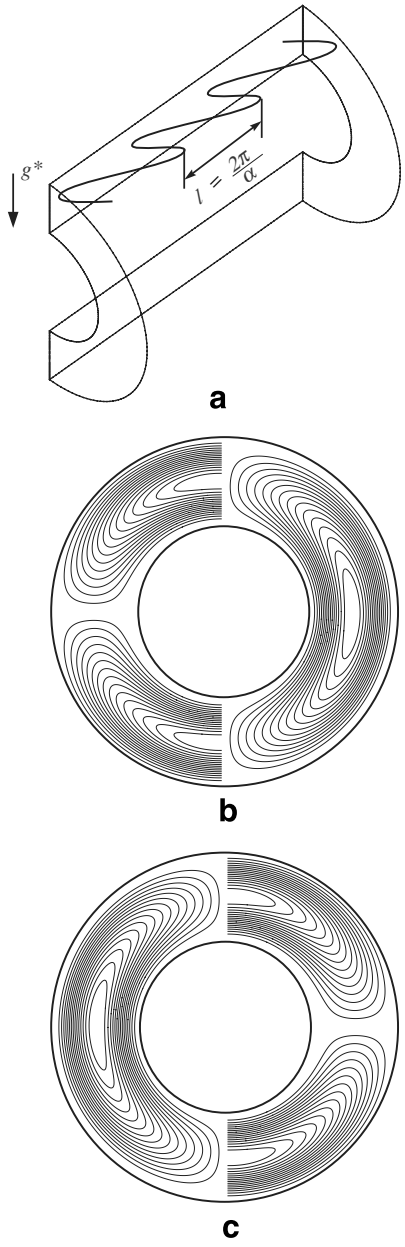

Fig. 2. Schematic figures of disturbance modes. (a) Three-dimensional oscillation of disturbances with wave number α. (b), (c) Disturbance flow and temperature fields of the cross section of the annulus, where the streamlines are on the right side and the isotherms on the left side. (b) s-mode, (c) a-mode.

$$\begin{pmatrix} u_r \\ u_\theta \\ u_z \\ T \end{pmatrix} = \begin{pmatrix} U_r \\ U_\theta \\ 0 \\ T \end{pmatrix} + \begin{pmatrix} \hat{u}_r \\ \hat{u}_\theta \\ \hat{u}_z \\ \hat{T} \end{pmatrix} \exp\{i(\alpha z - \omega t)\}, \tag{15}$$

where α is a wave number and ω is a complex frequency. The real part ω_r and the imaginary part ω_i denote the angular frequency and the linear growth rate of the disturbance, respectively.

The steady solution is unstable if $\omega_i > 0$ and the disturbance grows with time. There are two types of instability. One is that the steady solution is unstable in regard to a stationary disturbance and it bifurcates to another steady solution if $\omega_r = 0$ when ω_i vanishes. The other is that the steady solution is unstable in regard to an oscillatory disturbance and it bifurcates to a periodic solution with an angular frequency of ω_r if $\omega_r \neq 0$ when $\omega_i = 0$. In addition, the disturbance with $\alpha = 0$ forms the two-dimensional disturbance flow field, while that with $\alpha \neq 0$ forms the three-dimensional one. Schematic figure of oscillating disturbance with the wave number α and the corresponding wave length $l = 2\pi/\alpha$ is depicted in Fig. 2(a).

Substituting Eq. (15) into Eqs. (2)–(6), then subtracting the steady-state equations from the resultant equations, using the penalty-function method for the pressure also here and dropping the non-linear terms of the disturbance, we obtain the following linearized equations for the disturbance as:

$$\begin{aligned} &-i\omega\hat{u}_r + U_r\frac{\partial \hat{u}_r}{\partial r} + \hat{u}_r\frac{\partial U_r}{\partial r} + \frac{U_\theta}{r}\frac{\partial \hat{u}_r}{\partial \theta} + \frac{\hat{u}_\theta}{r}\frac{\partial U_r}{\partial \theta} - \frac{2U_\theta\hat{u}_\theta}{r} \\ &= \frac{1}{\epsilon}\frac{\partial}{\partial r}\left\{\frac{\partial}{\partial r}(r\hat{u}_r) + \frac{\partial \hat{u}_\theta}{\partial \theta} + r\alpha\hat{u}_z\right\} + PrRa\hat{T}\cos\theta \\ &\quad + Pr\left(\frac{\partial^2 \hat{u}_r}{\partial r^2} + \frac{1}{r}\frac{\partial \hat{u}_r}{\partial r} + \frac{1}{r^2}\frac{\partial^2 \hat{u}_r}{\partial \theta^2} - \alpha^2\hat{u}_r - \frac{2}{r^2}\frac{\partial \hat{u}_\theta}{\partial \theta} - \frac{\hat{u}_r}{r^2}\right), \end{aligned} \tag{16}$$

$$\begin{aligned} &-i\omega\hat{u}_\theta + U_r\frac{\partial \hat{u}_\theta}{\partial r} + \hat{u}_r\frac{\partial U_\theta}{\partial r} + \frac{U_\theta}{r}\frac{\partial \hat{u}_\theta}{\partial \theta} + \frac{\hat{u}_\theta}{r}\frac{\partial U_\theta}{\partial \theta} - \frac{\hat{u}_r U_\theta + U_r\hat{u}_\theta}{r} \\ &= \frac{1}{\epsilon r}\frac{\partial}{\partial \theta}\left\{\frac{\partial}{\partial r}(r\hat{u}_r) + \frac{\partial \hat{u}_\theta}{\partial \theta} + r\alpha\hat{u}_z\right\} - PrRa\hat{T}\sin\theta \\ &\quad + Pr\left(\frac{\partial^2 \hat{u}_\theta}{\partial r^2} + \frac{1}{r}\frac{\partial \hat{u}_\theta}{\partial r} + \frac{1}{r^2}\frac{\partial^2 \hat{u}_\theta}{\partial \theta^2} - \alpha^2\hat{u}_\theta + \frac{2}{r^2}\frac{\partial \hat{u}_r}{\partial \theta} - \frac{\hat{u}_\theta}{r^2}\right), \end{aligned} \tag{17}$$

$$\begin{aligned} &-i\omega\hat{u}_z + U_r\frac{\partial \hat{u}_z}{\partial r} + \frac{U_\theta}{r}\frac{\partial \hat{u}_z}{\partial \theta} \\ &= \frac{1}{\epsilon}\left\{-\alpha\frac{\partial}{\partial r}(r\hat{u}_r) - \alpha\frac{\partial \hat{u}_\theta}{\partial \theta} - r\alpha^2\hat{u}_z\right\} \\ &\quad + Pr\left(\frac{\partial^2 \hat{u}_z}{\partial r^2} + \frac{1}{r}\frac{\partial \hat{u}_z}{\partial r} + \frac{1}{r^2}\frac{\partial^2 \hat{u}_z}{\partial \theta^2} - \alpha^2\hat{u}_z\right), \end{aligned} \tag{18}$$

$$\begin{aligned} &-i\omega\hat{T} + U_r\frac{\partial \hat{T}}{\partial r} + \hat{u}_r\frac{\partial T}{\partial r} + \frac{U_\theta}{r}\frac{\partial \hat{T}}{\partial \theta} + \frac{\hat{u}_\theta}{r}\frac{\partial T}{\partial \theta} \\ &= \frac{\partial^2 \hat{T}}{\partial r^2} + \frac{1}{r}\frac{\partial \hat{T}}{\partial r} + \frac{1}{r^2}\frac{\partial^2 \hat{T}}{\partial \theta^2} - \alpha^2\hat{T}. \end{aligned} \tag{19}$$

The boundary conditions for ($\hat{u}_r, \hat{u}_\theta, \hat{u}_z$) are the same as Eqs. (8) and (9), while the condition for $\hat{T}$ is written as

$$\widehat{T} = 0 \quad \text{at } r = \frac{A}{2},\ \frac{A}{2}+1. \tag{20}$$

In addition, since the non-linear steady-state solutions have the symmetry conditions of Eq. (14), the linear stability of such solutions can be analyzed by considering the following symmetric (s-mode) and asymmetric (a-mode) modes of the disturbances separately. Then, the symmetry and asymmetry conditions for these two modes are written as s-mode:

$$\frac{\partial \widehat{u}_{\mathrm{r}}}{\partial \theta} = \widehat{u}_\theta = \frac{\partial \widehat{u}_z}{\partial \theta} = \frac{\partial \widehat{T}}{\partial \theta} = 0 \quad \text{at } \theta = 0, \pi. \tag{21}$$

a-mode

$$\widehat{u}_{\mathrm{r}} = \frac{\partial \widehat{u}_\theta}{\partial \theta} = \widehat{u}_z = \widehat{T} = 0 \quad \text{at } \theta = 0, \pi. \tag{22}$$

We can derive the above conditions considering the parities of the velocity and temperature in Eqs. (16)–(19). For instance, $(\widehat{u}_{\mathrm{r}}, \widehat{u}_z, \widehat{T})$ are odd functions of θ and $\widehat{u}_\theta$ is an even function in Eq. (22). Introducing the parities of the disturbance of a-mode in Eqs. (16)–(19) and considering the parities of steady solution such that (U_{r}, T) are even functions and U_θ is an odd function of θ, we can see the equation system consistent. It should be noted that the flow of disturbances does not pass through the vertical center-plane for the s-mode, while it does pass through the plane for the a-mode, where the schematic flow and temperature fields of the cross section of the annulus are depicted in Fig. 2(b) and (c).

3. Numerical method

Numerical calculations are carried out by utilizing a spectral element method [12,13]. The spectral element method has both the generality of the finite element method and the accuracy of the classical spectral method.

In the spectral element method, the actual calculation domain of $A/2 \leqslant r \leqslant A/2+1$ and $0 \leqslant \theta \leqslant \pi$ is broken up into K elements, where the computational domain for θ is reduced by half because of the symmetry and asymmetry conditions as Eqs. (14), (21) and (22). Here we break the domain into three elements in order to be more dense in the top of the annulus such as (1) $0 \leqslant \theta \leqslant \pi/6$, (2) $\pi/6 \leqslant \theta \leqslant \pi/3$ and (3) $\pi/3 \leqslant \theta \leqslant \pi$, where the range of r is fixed as $A/2 \leqslant r \leqslant A/2+1$. Each element is mapped from the physical (r,θ) space to the local $(\overline{r},\overline{\theta})$ co-ordinate system whose ranges are $[-1,1]$. For example, the co-ordinate transformations from (r,θ), defined on the interval $[r_a^k, r_b^k], [\theta_a^k, \theta_b^k]$ in the kth element, to $(\overline{r},\overline{\theta})$ are carried out by the following equations as:

$$\overline{r} = \frac{2}{r_b^k - r_a^k}(r - r_a^k) - 1, \quad \overline{\theta} = \frac{2}{\theta_b^k - \theta_a^k}(\theta - \theta_a^k) - 1. \tag{23}$$

The velocity and temperature are expanded by high-order Lagrangian interpolants as

$$\begin{pmatrix} u_{\mathrm{r}}^k(\overline{r},\overline{\theta}) \\ u_\theta^k(\overline{r},\overline{\theta}) \\ u_z^k(\overline{r},\overline{\theta}) \\ T^k(\overline{r},\overline{\theta}) \end{pmatrix} = \sum_{m=0}^{N}\sum_{n=0}^{N} \begin{pmatrix} u_{rmn}^k \\ u_{\theta mn}^k \\ u_{zmn}^k \\ T_{mn}^k \end{pmatrix} h_m(\overline{r}) h_n(\overline{\theta}), \tag{24}$$

where h_m is the Nth order Lagrange interpolants through $(N+1)$ Gauss–Legendre–Lobatto points in the k-th element.

Substituting the expansions of Eq. (24) into the weak forms of both the steady-state and disturbance equations and also using the Galerkin method, we obtain a set of algebraic equations for the coefficients of the expansions. We use a mapping array method [13] to construct the system matrix from the element matrices. The set of algebraic equations for the steady solution are solved numerically by the Newton–Raphson method. On the other hand, the set of algebraic equations for the stability of the steady solution constitutes a generalized eigenvalue problem in a matrix form as

$$\mathbf{Aa} = \mathrm{i}\omega\mathbf{Ba}, \tag{25}$$

where $\mathbf{a}$ is a vector of expansion coefficients, and $\mathbf{A}$ and $\mathbf{B}$ are the real general matrices arising from the right-hand side and left-hand side of Eqs. (16)–(19), respectively. The eigenvalue ω, with maximum imaginary part which is called a most unstable mode, determines the stability characteristics of the steady solution and the corresponding eigenvector represents the flow and temperature fields of the disturbance. This kind of stability analysis based on the spectral element method and the eigenvalue problem have been carried out by Adachi and Uehara [15] for flow in a complex geometry. A computation of all the eigenvalues would be prohibitive. It seems plausible that the most unstable mode must be located by looking only at the some eigenvalues with smallest absolute values. This can be easily done by using a simultaneous inverse iteration method [14]. Therefore, the eigenvalue problem is solved numerically by the simultaneous inverse iteration method. When the angular frequency ω_{r} is not zero and has a large value, however, the most unstable mode may not be included in these eigen values with smallest absolute ones, so we crosscheck in places by calculating all eigen values by the QR method.

4. Results

We investigate the three-dimensional linear stability of the two-dimensional steady solutions of the crescent-shaped ones over a wide range of aspect ratio $1 \leqslant A \leqslant 20$ and $Pr = 0.71$.

4.1. Numerical check

First, we check the numerical convergence of our calculations. All the numerical calculations are done with double precisions. According to the previous studies [2,7],

Table 1
Convergence of the eigenvalues, $\omega = \omega_r + i\omega_i$, for the truncation parameters N

	N	s-mode		a-mode	
		ω_r	ω_i	ω_r	ω_i
$A = 5$, $\alpha = 3.05$, $Ra = 1900$	8	0.0	0.521230	0.0	−0.827790
	10	0.0	0.520719	0.0	−0.828506
	12	0.0	0.520713	0.0	−0.828498
	Choi and Kim [7]	0.0	0.573		
$A = 2$, $\alpha = 3.45$, $Ra = 100{,}000$	18	108.690	1.68087	119.224	2.57896
	20	108.736	1.47898	119.352	2.30632
	22	108.742	1.43442	119.423	2.27941

the critical Rayleigh number might be $O(10^5)$ for a relatively small aspect ratio less than $A \sim 2$, while $O(10^3)$ for moderate and large values of aspect ratio greater than $A \sim 2$. So, we calculate the eigenvalues for $A = 2$, $Ra = 100{,}000$, $\alpha = 3.45$ and $A = 5$, $Ra = 1900$, $\alpha = 3.05$ to check the convergence of the eigenvalues for some truncation parameters N. In calculations using the simultaneous inverse iteration method, the 100 smallest eigenvalues of the matrix are calculated iteratively for $A = 2$, $Ra = 100{,}000$, while the 30 smallest eigenvalues are calculated for $A = 5$, $Ra = 1900$.

The eigenvalues are given in Table 1 for the truncation parameters N. It is found that $N = 10$ is enough to obtain four significant digits for $A = 5$ and $Ra = 1900$. The eigenvalue is compared with the result of Choi and Kim [7]. They obtained the linear growth rate from the numerical simulation on the initial-value problem of the linearized disturbance equations to the Navier–Stokes equations. Our result is in reasonable agreement with that of Choi and Kim. On the other hand, in the case of a larger value of the Rayleigh number, $N = 20$ is needed to obtain three to four significant digits for $A = 2$ and $Ra = 100{,}000$. Therefore, the truncation parameter are hereafter taken as $N = 20$ for $Ra > O(10^4)$ and $M = 10$ for $Ra < O(10^3)$ to keep three to four significant digits.

4.2. Linear stability

We show the linear neutral stability curves as a function of the wave number α, where the maximum linear growth rate ω_i changes from a negative value to a positive one. When the neutral curve has a local minimum, we define the point as the critical Rayleigh number Ra_c and the critical wave number α_c.

We show the neutral stability curve for $A = 2$ and 3 as typical examples. Fig. 3 indicates the neutral curves obtained for $A = 2$. We can see that the neutral curve of the a-mode is smaller than one of the s-mode, and has a local minimum. So, the a-mode gives the critical Rayleigh number as $Ra_c = 25{,}260$ at $\alpha_c = 3.45$. Then, the angular frequency is $\omega_r = 62.76$. Therefore, the crescent-shaped convection becomes unstable for the oscillatory disturbance of the a-mode, and the resultant convection due to the instability is a three-dimensional oscillatory flow passing through the vertical center-plane. On the other hand, the neutral curve for $A = 3$ is depicted in Fig. 4. It is

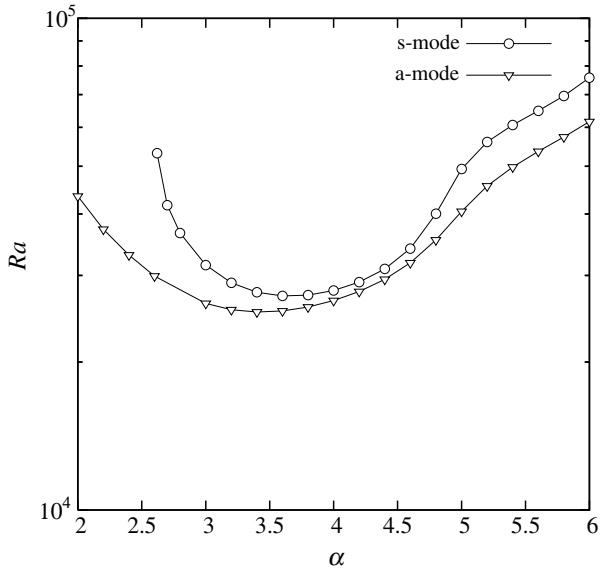

Fig. 3. Neutral stability curve for $A = 2$.

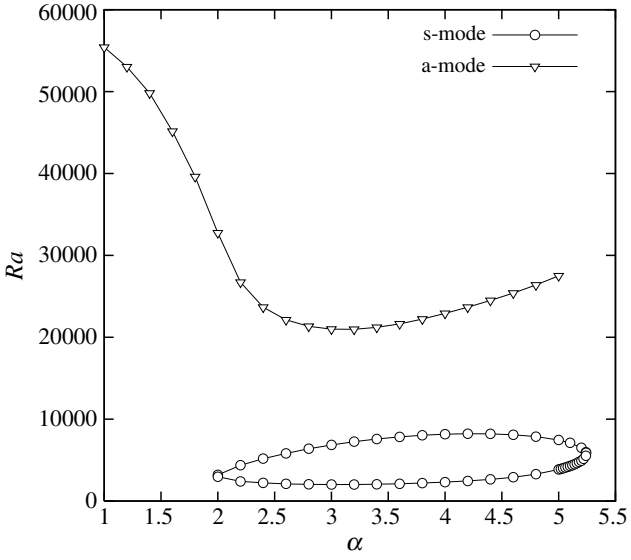

Fig. 4. Neutral stability curve for $A = 3$.

emphasized that there is a closed region of the curve for the s-mode in the range of $2.0 \leqslant \alpha \leqslant 5.24$ and the curve is lower than that of the a-mode. So, the s-mode gives the critical Rayleigh number as $Ra_c = 2009$ at $\alpha_c = 3.08$. Then, the angular frequency is $\omega_r = 0$. Therefore, the crescent-shaped convection becomes unstable for the stationary disturbance of the s-mode and the resultant convection is a three-dimensional steady flow.

Furthermore, we calculate the critical Rayleigh numbers for other values of the aspect ratio A and show them as transition lines in Fig. 5. The solid lines with plots of circles and triangles show our results, while the dot-dashed lines AB, CD and EF are the transition lines suggested by Powe et al. [2], where a two-dimensional oscillatory flow occurs above AB, a three-dimensional oscillatory one above CD and a two-dimensional multicellular one above EF. And the results of Choi and Kim [7] are indicated by squares. The critical Rayleigh number obtained in the present study shows good agreement with the results of Choi and Kim on the transition line for the aspect ratio greater than $A \sim 2$. It is clear that the exchange of stabilities [16] are valid on the line and a three-dimensional steady flow occurs after the transition, which is different from the transition line EF of Powe et al. [2]. Since the critical Rayleigh number is $Ra_c = 1723$ at $\alpha = 3.02$ for $A = 20$ in this study, the present line tends to an asymptotic value of the critical Rayleigh number for the Rayleigh–Bénard convection, $Ra_c = 1707.8$ and $\alpha_c = 3.12$, as $A \to \infty$. This means that the roll type convection whose axes are perpendicular to the axis of the annulus occurs for $A \to \infty$ because of $\alpha_c \neq 0$.

On the other hand, when the Rayleigh number increases abruptly at $A \sim 2$, Choi and Kim reported that they could not obtain the critical Rayleigh number for $A < 2.1$. We can understand the reason from the neutral curve around $A \sim 2$. It is expected that the closed neutral curve in the wave number-Rayleigh number plane as seen in Fig. 4

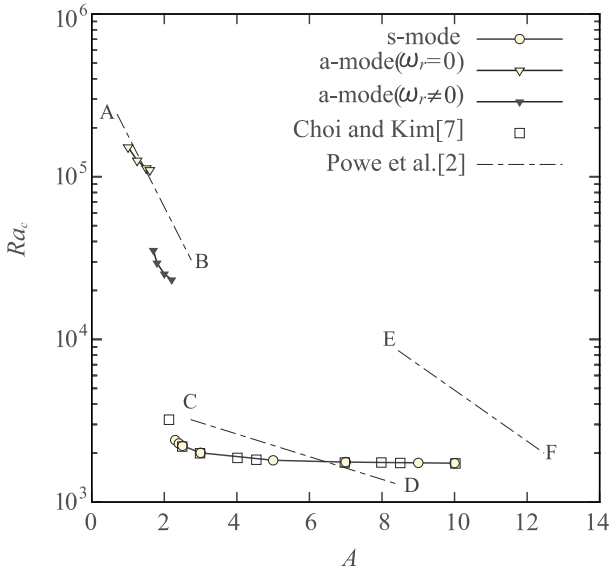

Fig. 5. Critical Rayleigh number Ra_c as a function of the aspect ratio A.

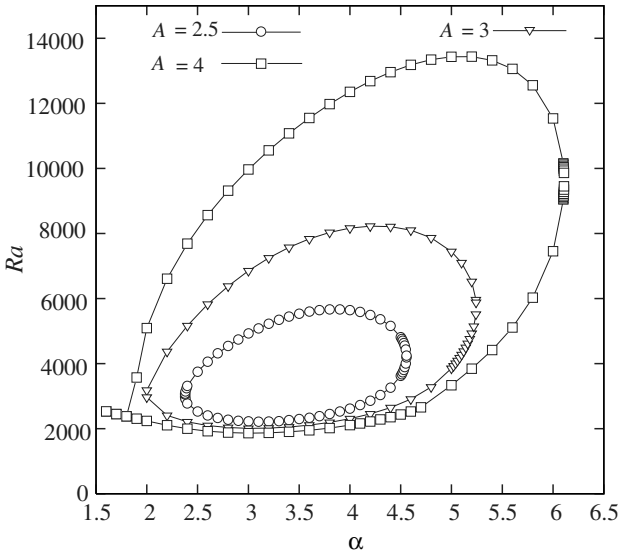

Fig. 6. Neutral curves with closed region.

might shrink to a point and subsequently disappear as the aspect ratio decreases to the value of $A \sim 2$. This leads to the discontinuous increase of the critical Rayleigh number near $A \sim 2$. Actually, it is confirmed that the closed region shrinks as the aspect ratio decreases as seen in Fig. 6 and the critical aspect ratio where the closed region disappears is obtained as $A = 2.2$ in this study. Moreover, there are two different curves of the critical Rayleigh number for $1 \leqslant A \leqslant 2.2$ depending on the angular frequency ω_r of the disturbance. Namely, one is a curve above which the crescent-shaped convection bifurcates to a three-dimensional steady flow indicated by open triangles, and the other is one above which the crescent-shaped convection bifurcates to a three-dimensional oscillatory flow indicated by filled triangles in Fig. 5. These lines are different from the transition line AB suggested by Powe et al. [2].

In order to conclude these complicated bifurcation phenomenon, we propose the new transition lines, i.e., (i) for $1 \leqslant A \leqslant 1.6$, the two-dimensional crescent-shaped convection becomes unstable for the steady three-dimensional disturbances and the resultant convection is a three-dimensional steady one, (ii) for $1.7 \leqslant A \leqslant 2.2$, the two-dimensional convection becomes unstable for the oscillatory three-dimensional disturbances and the resultant flow is a three-dimensional oscillatory one, and (iii) for $A \geqslant 2.3$, the crescent-shaped convection becomes unstable for the steady three-dimensional disturbances and the resultant convection is a three-dimensional steady one. In addition, the resultant convection for $1 \leqslant A \leqslant 2.2$ passes through the vertical symmetry plane because the instability mode is the disturbances of the a-mode, while the resultant flow is symmetric with the vertical plane for $A \geqslant 2.3$.

4.3. Flow field of disturbances

As we have seen, the transition lines change depending on a mode of the most unstable disturbance. In this paper,

however, not carried out the full three-dimensional numerical simulation, we cannot visualize the exact subsequent flow patterns after the transition. So, we show the disturbance flow fields on the transition lines to investigate the nature of the hydrodynamic instability. Flow fields of the most unstable disturbance mode are obtained from the eigenvector of the eigenvalue problem. We display the flow fields of the disturbance by an vector field of the eigenvector at the criticality. The range of the z-direction in the figure is $0 \leqslant z \leqslant 3l$, where $l = 2\pi/\alpha$ is a wave length in the z-direction of the disturbance.

We show the spatial structure of the disturbance flow field for $A = 2$ at the critical state as $Ra_c = 25{,}260$ and $\alpha_c = 3.45$ in Fig. 7 together with the corresponding steady-state solutions of the crescent-shaped convection. In Fig. 7(a), the streamlines of the steady-state solutions at the critical state are on the right side, while the isotherms are on the left side. It is seen that there is the crescent-shaped convection with the center on $\theta \sim 60^\circ$ from the top and it affects the isotherms being thinner at the bottom of the inner cylinder and at the top of the outer cylinder, respectively. This means that the heat transfer is enhanced at these locations, because the thermal boundary layer is also thin there. The vector field of the disturbance velocity at the cross section of $r = A + 0.5$ is shown in Fig. 7(b). The disturbance flow reaches near the bottom region of the annulus with a certain magnitude. This means that the disturbance flow field destabilizes the crescent-shaped convection overall the annulus. In addition, the distribution of the disturbance velocity is similar to the case of $A = 1$.

On the other hand, the steady-state solutions and the spatial structure of the disturbance for $A = 3$ at the critical state as $Ra_c = 2009$ and $\alpha_c = 3.08$ are shown in Fig. 8. It is evident that there is the crescent-shaped convection with the center on $\theta \sim 90^\circ$ and it does not affect the isotherms, because the Rayleigh number is relatively small compared

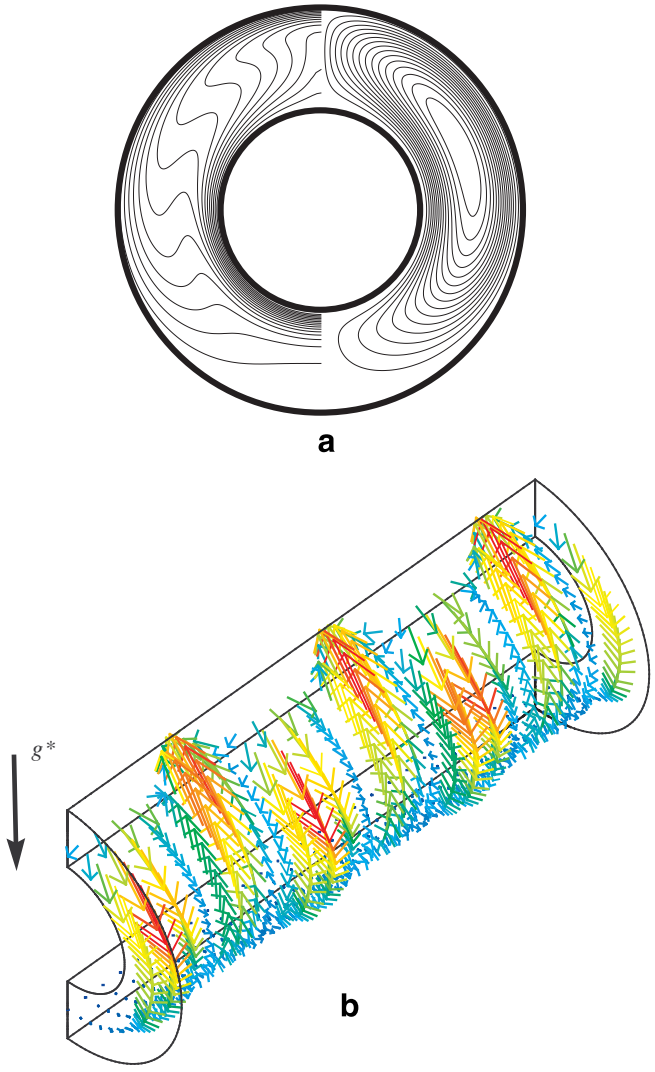

Fig. 7. Flow fields at the critical state for $A = 2$: (a) stream-lines of the crescent-shaped convection of the right side and isotherm on the left side and (b) vector field of the disturbance velocity.

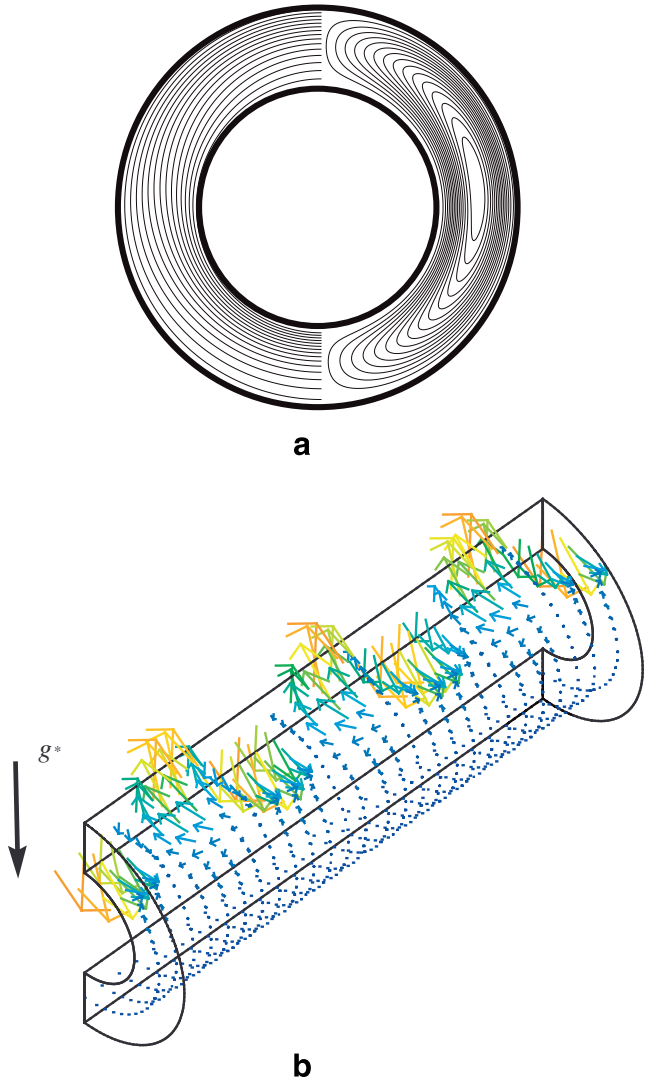

Fig. 8. Flow fields at the critical state for $A = 3$: (a) stream-lines of the crescent-shaped convection of the right side and isotherm on the left side and (b) vector field of the disturbance velocity.

with the case of $A = 2$. Therefore, the isotherms are almost concentric circles, so the heat transfer is by thermal conduction. Moreover, the vector field of the disturbance velocity as seen in Fig. 8(b) concentrates at the top region of the annulus and the disturbance flow does not reach the bottom region of the annulus, which is in contrast to the case of $A = 2$. This is mainly due to the difference of the disturbance mode. As mentioned previously, the disturbance mode which destabilizes the crescent-shaped convection is the a-mode for $A \leqslant 2.2$, and the s-mode for $A \geqslant 2.3$.

5. Concluding remarks

Linear stability of two-dimensional natural convections between two concentric horizontal cylinders with regard to infinitesimal three-dimensional disturbances has been investigated for a fluid of $Pr = 0.71$. The eigenvalue problem has been constituted by successfully applying the linear stability theory. We summarize the main conclusions as follows.

1. The critical Rayleigh numbers where the basic two-dimensional flow, called a crescent-shaped convection, loses its stability with respect to three-dimensional disturbances have been obtained over a wide range of aspect ratio $1 \leqslant A \leqslant 20$. It is found that the crescent-shaped convection always becomes unstable for the three-dimensional disturbances with $\alpha \neq 0$, and the resultant flow due to the instability is a three-dimensional convection.
2. We have proposed new transition lines of Ra_c which consist of three lines as a function of aspect ratio A. (i) for $1 \leqslant A \leqslant 1.6$, the crescent-shaped convection bifurcates to a three-dimensional steady one without the symmetry in the vertical center-plane, (ii) for $1.7 \leqslant A \leqslant 2.2$, the crescent-shaped convection bifurcates to a three-dimensional oscillatory one without the symmetry in the vertical plane, and (iii) for $A \geqslant 2.3$, the crescent-shaped convection bifurcates to a three-dimensional steady one with the symmetry in the vertical plane.
3. It is found that the disturbance flow field which destabilizes the crescent-shaped convection reaches near the bottom of the annulus if the disturbance mode is the a-mode for $A \leqslant 2.2$, while is stagnant in the top region of the annuls if the disturbance mode is the s-mode for $A \geqslant 2.3$.

Acknowledgements

Part of the results in this work were obtained using supercomputing resources at Information Synergy Center, Tohoku University and at the Supercomputer Center, Institute for Solid State Physics, University of Tokyo. We also thank Mr. J. Kuhn for his helpful comments.

References

[1] E.H. Bishop, C.T. Carley, R.E. Powe, Natural convective oscillatory flow in cylindrical annuli, Int. J. Heat Mass Transfer 11 (1968) 1741–1751.
[2] R.E. Powe, C.T. Carley, E.H. Bishop, Free convective flow patterns in cylindrical annuli, Trans. ASME J. Heat Transfer 91 (1969) 310–314.
[3] R.E. Powe, C.T. Carley, S.L. Carruth, A numerical solution for natural convection in cylindrical annuli, Trans. ASME J. Heat Transfer (1971) 210–220.
[4] T.H. Kuehn, R.J. Goldstein, An experimental and theoretical study of natural convection in the annulus between horizontal concentric cylinders, J. Fluid Mech. 74 (1976) 695–719.
[5] J.S. Yoo, Dual steady solutions in natural convection between horizontal concentric cylinders, Int. J. Heat Fluid Flow 17 (1996) 587–593.
[6] J. Mizushima, S. Hayashi, T. Adachi, Transitions of natural convection in a horizontal annulus, Int. J. Heat Mass Transfer 44 (2001) 1249–1257.
[7] J.Y. Choi, M.U. Kim, Three-dimensional linear stability of natural convective flow between concentric horizontal cylinders, Int. J. Heat Mass Transfer 36 (1993) 4173–4180.
[8] M.P. Dyko, K. Vafai, A.K. Mojtabi, A numerical and experimental investigation of stability of natural convective flows within a horizontal annulus, J. Fluid Mech. 381 (1999) 27–61.
[9] G. Labonia, G. Gui, Natural convection in a horizontal concentric cylindrical annulus: oscillatory flow and transition to chaos, J. Fluid Mech. 375 (1998) 179–202.
[10] A.J. Baker, Finite Element Computational Fluid Mechanics, McGraw-HILL, 1985 (Chapter 2).
[11] J.N. Reddy, On penalty function methods in the finite-element analysis of flow problems, Int. J. Numer. Methods Fluids 2 (1982) 151–171.
[12] A.T. Patera, A spectral element method for fluid dynamics: laminar flow in a channel expansion, J. Comput. Phys. 54 (1984) 468–488.
[13] G.E. Karniadakis, S.J. Sherwin, Spectral/hp Element Methods for CFD, Oxford University Press, 1999 (Section2).
[14] A. Fortin, M. Jardak, J.J. Gervais, R. Pierre, Old and new results on the two-dimensional Poiseuille flow, Int. J. Comput. Phys. 115 (1994) 455–469.
[15] T. Adachi, H. Uehara, Linear stability analysis of flow in a periodically grooved channel, Int. J. Numer. Method Fluids 41 (2003) 601–613.
[16] P.G. Drazin, W.H. Reid, Hydrodynamic Stability, Cambridge University Press, 1981 (Section 2).